Biologically Plausible Information Propagation in a CMOS Integrate-and-Fire Artificial Neuron Circuit with Memristive Synapses

Biologically Plausible Information Propagation in a CMOS Integrate-and-Fire Artificial Neuron Circuit with Memristive Synapses

Lorenzo Benatti[1], Tommaso Zanotti[1], Daniela Gandolfi[2,3], Jonathan Mapelli[2,3], Francesco Maria Puglisi[1,3]
[1]Dipartimento di Ingegneria "Enzo Ferrari", Via. P. Vivarelli 10/1, 41125 Modena, Italy
[2]Dipartimento di Scienze Biomediche, Metaboliche e Neuroscienze, Via G. Campi 287, 41125 Modena, Italy
[3] Centro Interdipartimentale di Neuroscienze e Neurotecnologie
Università degli Studi di Modena e Reggio Emilia
Corresponding author email: francescomaria.puglisi@unimore.it phone: +39-059-2056352

Abstract— **Neuromorphic circuits based on spikes are currently envisioned as a viable option to achieve brain-like computation capabilities in specific electronic implementations while limiting power dissipation given their ability to mimic energy efficient bio-inspired mechanisms. While several network architectures have been developed to embed in hardware the bio-inspired learning rules found in the biological brain, such as the Spike Timing Dependent Plasticity, it is still unclear if hardware spiking neural network architectures can handle and transfer information akin to biological networks. In this work, we investigate the analogies between an artificial neuron combining memristor synapses and rate-based learning rule with biological neuron response in terms of information propagation from a theoretical perspective. Bio-inspired experiments have been reproduced by linking the biological probability of release with the artificial synapses conductance. Mutual information and surprise have been chosen as metrics to evidence how, for different values of synaptic weights, an artificial neuron allows to develop a reliable and biological resembling neural network in terms of information propagation and analysis.**

I. Introduction

Neuromorphic technologies have been designed to support large-scale Spiking Neural Networks (SNNs) encompassing bio-inspired mechanisms. Differently from conventional artificial intelligence systems, these networks base their activity on the transfer of binary units (spikes) through synaptic contacts. These latter in turn can undergo persistent changes of their strength upon specific patterns of stimulation. The modifications expressed by synaptic contacts following the induction of long-term plasticity [1-2] can be reliably reproduced by memristors [3-5], which can been designed to change their conductance according to their past activity [6]. In this respect, recent advancements in memristive device technology development brought them closer to full integration in standard CMOS platforms, which is per se a though challenge as these devices must fulfil very stringent requirements for integration with current integrated circuits. Among these requirements are integration densities up to 1 Gigabyte/mm^2, writing voltages <3 V, switching energy <10 pJ, switching time <10 ns, writing endurance >10^{10} cycles (or full potentiation/depression cycles), dynamic range >10, and low conductance fluctuations over time if no bias is applied (< 10% for > 10 years) [7]. Notably, some memristive devices have fulfilled such stringent criteria [7-8], but still exhibit high manufacturing costs despite the simplicity of the individual memristive cell due to the need of additional elements (series transistor, selector, or resistor) and to specific beyond-CMOS back-end-of-line (BEOL) interconnects. Still, these devices are gradually triggering the interest of the semiconductor industry and are currently considered as frontrunners in the race to realize a CMOS-compatible, cost-effective synaptic element for hardware SNNs.

Interestingly, several network architectures have been developed to embed in hardware the bio-inspired learning rules that are required to exploit SNNs functionality, such as the Spike Timing Dependent Plasticity, Rate-Based Plasticity, or the Bienestock-Cooper-Munro learning rule [6]. Nevertheless, while a significant amount of work has been published in this domain, it is still unclear if currently proposed neuromorphic hardware architectures for SNNs have the capacity to handle and transfer information in a way that resembles what happens in the corresponding biological networks. In a neuronal microcircuit, in fact, the information is exchanged between neurons in the form of input spike series that are conveyed as output temporal spikes series. Therefore, the amount of transferred information can be estimated by looking at the input-output relationship which is computed by analysing the stimulus patterns and the neural responses. This dependency can be formalized in several ways like tuning [9-10], gain [11] or selectivity curves [12-13], and these approaches allow to provide quantitative estimates of the information content independently from the neural code. The language employed by neurons to communicate can be cracked by adopting parameters of communication and information theory [14]. Among these, the Mutual Information (MI) has been already adapted to neuroscience to estimate the information transmitted by circuits [15], neurons [16] or single synapses [17] without specific knowledge of neural code semantic. The MI is directly derived from the response and noise entropy [18] which are correlated to the variability of responses to different inputs or to the same input. Given this premise, the calculation of MI allows to evaluate the capacity of a neuronal system to separate different inputs and thus transmitting information [19-20]. For this reason, MI has been used consistently in neuroscience to show the modalities of information

propagation in biological neural networks. On the other hand, much of the efforts in neuromorphic electronics has been devoted to the design, development, and implementation of artificial CMOS [21] or memristive [22] neurons and either CMOS or memristive synapses [23-25] in circuits that embed specific learning rules and electrophysiological properties, paying less or no attention to the overall performance of the system under investigation from the standpoint of information transmission. In fact, understanding whether currently proposed artificial SNNs can at least qualitatively replicate the extremely efficiency with which biological networks handle and transfer information represents an important step toward the development of brain-inspired and ultra-low power artificial processing systems.

In this work, we provide for the first time an in-depth analysis of the information transmission in a SNN that encompasses CMOS Leaky Integrate and Fire (LIF) neurons and memristive synapses by focusing on how MI is transmitted through the network. Specifically, we focus on a simplified network with the neuron circuit mimicking a cerebellar granule cell, found to be the optimal benchmark to calculate MI [26]. In fact, in the case of the cerebellar granule cell, the input-output combination is particularly convenient given the small amount of dendrites (four) and the limited amount of inputs received, compared to the thousands of contacts received for instance by cortical and hippocampal pyramidal neurons. In addition, beside the few dendrites, granule cells when activated respond with a limited number of spikes (typically two or less [27]) confined in a narrow time window regulated by synaptic inhibition [28]. This peculiarity reduces the complexity of calculations and suggests the use of this microcircuit as a model to investigate changes in the transmission properties by internal or external agents. We compare how MI changes not only with the specific stimuli and input patterns but also how it evolves with changes induced by altering the synaptic strength (i.e., upon learning), finding a striking qualitative resemblance with the results found experimentally in biological networks [29-30] and in simulations with biologically realistic neurons [26]. This paper is organized as follows: in Section II we illustrate the methods used to compute specific quantities related to information propagation; in Section III we report the details of the synaptic device used in this study, clarifying how the latter were characterized and modelled; the details of the electronic neuron model are given as well; in Section IV we provide the details of the proposed artificial network and of the analogies and differences as compared to its biological counterpart; in Section V results are reported and discussed. Conclusions follow.

II. METHODS

Information theory has been extensively used in neuroscience to estimate the amount of information transmitted within neuronal circuits [14, 16, 20, 26] where a set of input stimuli can be correlated with output responses to estimate the information conveyed by neurons. The level of correlation primarily depends on the input variability which, in turn, is expanded by the number of afferent fibres. In the central nervous system there is a large variability in the number of input synapses a neuron can receive: from a few units (cerebellar granule cells [29]) to hundreds of thousands (200,000 in cerebellar Purkinje cells [30]). In terms of information transfer, only neurons with limited fan-in connections can be efficiently analysed avoiding the explosion of combinations according to the input space size. Following our recent work [31], we have simulated an artificial architecture composed of individual neurons with only four synaptic inputs, and the level of correlation was estimated by first dividing neuronal responses in temporal bins which were digitized in dependence on the presence of a spike. This discretization allowed to convert a spike train into a binary word of length $N = T/\Delta t$ (where Δt is the temporal bin and T is the spike train duration) containing only digital labels (where '0' means no spike and '1' means spike). Neurons respond to input stimuli with a variety of binary words generating the neuronal vocabulary that can be explored by varying input stimuli. The larger the vocabulary, the richer the conveyed information. However, an efficient communication is ensured by a correlation between input stimuli and output words. In information theory, two factors determine the amount of information a neuron conveys about its inputs, namely the response entropy (i.e., the neuronal vocabulary size) and the noise entropy (i.e., the reliability of responses when stimuli are given). The quantity that considers these two factors simultaneously by subtracting the noise entropy from response entropy is Shannon's Mutual Information (MI) which is measured in bits and can be calculated through the following equation:

$$MI(R,S) = MI(S,R) = H(R) - H(R|S) = \sum_{s\in S}\sum_{r\in R} p(s)p(r|s)\log_2\frac{p(r|s)}{p(r)} \quad (1)$$

where r and s are the response and the stimulus pattern, respectively; $p(r)$ and $p(s)$ are the probabilities that r or s occur within a single acquisition. Finally, $p(r|s)$ is the probability of obtaining the response pattern r given the stimulus pattern s.

The MI is intrinsically an average property of all inputs, and it can be interesting to decompose MI in the single stimulus contribution (Stimulus Specific Surprise - SSS) or even single spike contribution (Surprise per Spike – SpS). These two quantities can be computed as:

$$I(s^*) = SSS = \sum_r p(r|s^*)\log_2\frac{p(r|s^*)}{p(r)} \quad (2)$$

$$I_{perSpike}(s^*) = SpS = \frac{I(s^*)}{stimuls\ spike\ count} \quad (3)$$

Experimental issues associated to high data dimensionality limit the estimation of all the probabilities in the MI formula. Estimating the conditional entropy requires determining the response probability given any input stimulus. If the neural response shows sufficiently low variability, the response

probability can be assessed with a tractable amount of data [26, 31].

III. Synaptic Devices and Neuron Model

A. Synaptic Devices and Experiments

According to the configuration adopted for biological experiments [31] and simulations with biologically realistic neurons [26], we investigated how information is propagated in a cerebellar granule cell-like artificial CMOS neuron with 4 memristor-based synaptic inputs. In this respect, we run circuit simulations using Cadence Virtuoso software in which the response of the artificial CMOS neuron was abstracted by using a Verilog-A behavioural description of its constituent building blocks (as specified in Section III.B), while the characteristics of the memristive elements (i.e., the artificial synapses) were carefully reproduced by means of a compact model developed internally, i.e. the UniMORE RRAM compact model [32]. The latter is a physics-based compact model supported by the results of advanced multiscale simulations [33] that has been shown to reproduce both the quasi-static and the dynamic behavior of different memristor technologies with a single set of parameters [34] and considers the intrinsic device stochastic response, thermal effects, and random telegraph noise [35]. Specifically, the memristive elements adopted in this study are commercially available C-doped Self-Directed Channel (SDC) memristors by Knowm [36], available in a dual in-line package (DIP). These devices were chosen since, to the best of the authors' knowledge, they are the only commercially available packaged RRAM devices to date. This choice allows us showing that MI propagates through a SNN with CMOS LIF neurons and memristive synapses akin to what happens in biological networks and that such a behavior can be achievable with available commercial-grade RRAM devices, requiring no specific advancements in technology development.

As shown in Fig. 1a, the SDC memristor consists of a stack composed of W/Ge_2Se_3/Ag/Ge_2Se_3/SnSe/Ge_2Se_3:C/W, where Ge_2Se_3:C is the active layer [36]. During fabrication, the three layers below the top electrode (TE) are mixed and form the Ag source [36]. The SnSe layer acts as a barrier to avoid Ag saturation in the active layer and is responsible for the production of Sn ions and their migration into the active layer during the device initial operation (typically addressed as "forming"), which promotes Ag agglomeration in specific sites [36]. The details of the mechanism at the basis of the resistive switching in these devices is available in [36]. To fully capture the behavior of these devices in circuit simulations we carefully calibrated the parameters of the UniMORE RRAM compact model against experimental data, as elucidated in Fig. 1. The electrical measurements were performed using the Keithley 4200-SCS. To analyze and then model the behavior of the memristors we performed a sequence of quasi-static I–V measurements by applying voltages sweeping from -0.8 V to 0.4 V with a current compliance enforced to 10 µA by the Keithley 4200-SCS. These measurements drive the device to a low resistive state (LRS) with a SET operation (V > 0) and to a high resistive state (HRS) with an ensuing RESET operation

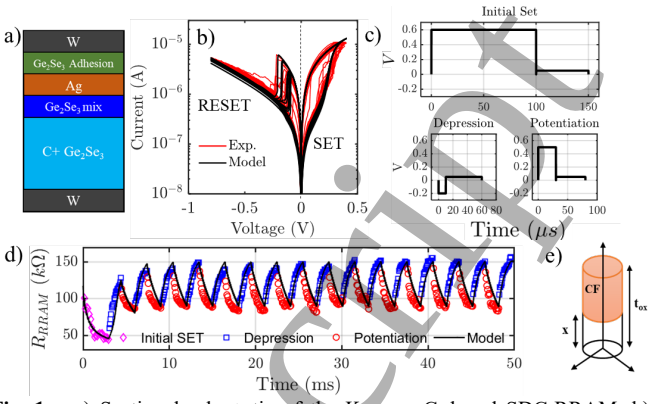

Fig. 1 – a) Sectional schematic of the Knowm C-doped SDC-RRAM. b) Experimental (red) and modelled (black) I-V characteristic, composed by a set (V > 0) and reset (V < 0) mechanism. c) Pulse waveforms used to potentiate and depress the memristor, including a 50ms read pulse. (d) Experimental (symbols) and simulated (solid line) pulsed response of the SDC-memristor when subject to sequences of potentiation (red circles) and depression (blue squares) pulses. The device is initially driven in LRS by means of 20 initial Set rectangular pulses. The resistance read after each pulse by means of a read pulse, is computed as (V_{READ}/I) − R_s (R_s = 10 kΩ series resistance). e) The I-V and pulsed characteristics of b) and d) are reproduced by modulating the CF barrier (x) of an equivalent oxide RRAM with an oxide thickness t_{ox} = 40nm.

(V < 0). Results are shown in Fig. 1b (red traces) and reveal that the RESET curves are characterized by an abrupt transition from the LRS to the HRS and a strong cycle-to-cycle variability of the switching voltage, while the SET operation is associated with a more predictable and gradual transition from HRS to LRS. Then, to experimentally evaluate the synaptic functionality of the memristors (i.e., the capability to respond to spike-like voltage stimuli rather than to quasi-static voltage sweeps) we designed a suitable pulsed voltage sequence (Fig. 1c) which gradually drives the device resistance toward higher or lower resistance (or, equivalently, conductance) states. In this experiment, a 10 kΩ resistor was connected in series with the device to prevent accidental current overshoots since the Keithley 4200-SCS does not support the enforcement of a current compliance when performing pulsed tests (the series resistor can then be removed in the actual circuit implementation). The device was initially driven in LRS by means of 20 rectangular pulses (V = 0.6 V, T = 100 µs – *Initial Set*). Then, long-term depression (LTD) and long-term potentiation (LTP) were obtained by applying trains of 20 depression pulses (V = − 0.2 V, T = 10 µs) followed by 20 potentiation pulses (V = 0.55 V, T = 30 µs). To evaluate the transition smoothness, each potentiation or depression pulse is followed by a small reading pulse (V_{READ} = 50 mV, T_{READ} = 50 µs) that is used to retrieve the evolution of the resistance values during LTD and LTP. Fig. 1c reports the resistance evolution for 15 identical depression-potentiation cycles, revealing that a smooth and reproducible synaptic analog behavior is achievable with these devices.

Although SDC-memristors are ion-conducting devices that change their resistance due to the movement of Ag^+ ions into the device structure [36], their behavior is well replicated (Fig. 1b,d – black traces) by the modulation of an equivalent conducting filament (CF) barrier (Fig. 1e) [32-35], that is the typical behavior of filamentary memristive devices. The

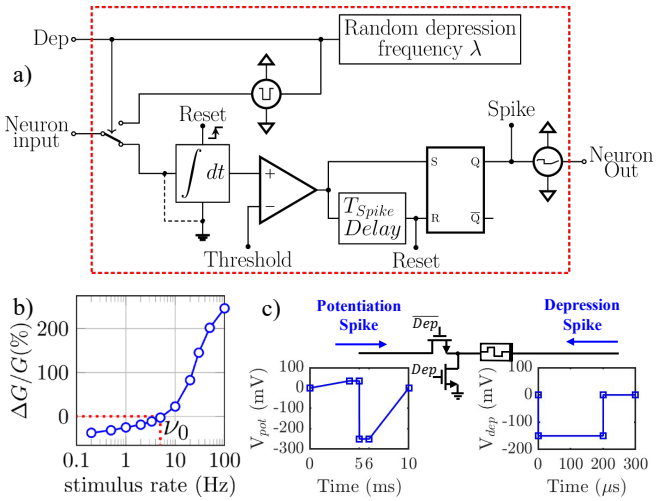

Fig. 2 – a) LIF neuron model. b) The synaptic plasticity is implemented by a rate-based learning rule where a presynaptic stimulation rate higher (lower) than ν_0 leads to the potentiation (depression) of the relative synapse. c) Spiking diagram for potentiation and depression.

barrier thickness (*x* in Fig. 1e*)* is in fact directly correlated to the memristor conductance, which represents the synaptic strength. Further details of the compact model and extracted parameters for this technology are reported in [6].

B. Neuron Model and Simulations

Fig. 2a shows the model of the Leaky Integrate-and-Fire (LIF) neuron [6] supporting a rate-dependent plasticity rule on the synaptic memristive devices that was designed and simulated in this work. In this neuron model, the input terminal (see *Neuron input* in Fig. 2a) is kept at virtual ground, and input spikes from presynaptic neurons are integrated into a capacitor. When the voltage across the capacitor passes a threshold, an output spike is generated at the neuron output, and after a predefined delay (i.e., T_{spike} *Delay* in Fig. 2a), the capacitor is discharged to reset the system to its initial state. The rate at which the capacitor charges depends both on the input spikes' rate and the presynaptic strength. Since the neuron is leaky, in absence of input spikes the capacitor discharges with an appropriate time constant. This feature mirrors the finding that biological neurons have a leaky membrane which contributes to depolarization when no spikes are fed at their inputs. The effect of the time constant value in the LIF model was already evaluated in [37] in which it is clearly shown that the presence of leakage provides enhanced noise-robustness of SNNs while decreasing sparsity in computation. This implies a trade-off between robustness and energy-efficiency in SNNs which can be optimized by mimicking the dynamics found in biological neurons, thus setting the LIF time constant close to the values used in biological neuron simulations.

The synaptic plasticity mechanism implemented in the neuron model is purely rate-based and depends only on the rate of the presynaptic stimulation. Thus, a high (low) rate of presynaptic stimulations lead to the potentiation (depression) of the associated synapse. In the adopted neuron model, this learning rule is implemented by appropriately designing the shape of the spike (see Fig. 2c) so that each presynaptic spike results in a small potentiation of the associated synaptic memristor device, and by introducing a back-spike which results in a small synaptic depression, see Fig. 2c. It is worth noting that this back-spike only serves the purpose of properly implementing the rate-based learning rule and is not related to the firing activity of the postsynaptic neuron and does not appear at its output.

When firing the back-spike from its input terminal, the postsynaptic neuron also outputs a *Dep* and a $\overline{Dep}$ control signals that are connected to the gate of two MOSFET devices (see Fig. 2a and 2c), which disconnect the synapses from their presynaptic neurons and connect their bottom electrodes to ground, see Fig. 2c.

When the neuron fires the back-spike, the propagation of information from the presynaptic neurons is therefore temporarily disabled. The occurrence of simultaneous presynaptic spikes and back-spikes is minimized by modelling the time interval between back-spikes as a random variable following a Poisson distribution (i.e., $\lambda = 1$ s was used in the simulations), and by designing a back-spike with a short duration. Since the back-spikes do not propagate any information, their shape can be designed with some degree of flexibility and can be adjusted as required. The back-spike used in the simulation is shown in Fig. 2c, and has a pulse width of 300 μs, which is much shorter than the presynaptic spike. The mean time interval between successive back-spikes determines the characteristic of the implemented rate-based learning rule. As shown in Fig. 2b, a stimulation rate ν_0 at which potentiation and depression effects balance out, leading to no average synaptic strength change, exists. Presynaptic stimulation rates higher than ν_0 result in a net synapse potentiation, while lower stimulation rates in a net depression, as shown in Fig. 2b. Although the spikes used in this work were designed to provide a system response in a similar timescale to that of biological neurons and to be compatible with the employed memristor technology, it is worth noting that the pulse shape and the parameters of the neuron circuit (e.g., threshold, integrator time constant) can be scaled appropriately to adapt the system response to satisfy possible application requirements, highlighting the flexibility of the electronic implementation of the bio-inspired neural network.

IV. Simulated Network

In order to understand whether the artificial SNN features information transmission properties akin to those found in biological systems we implemented a circuit that resembles the granule cell morphology, shown schematically in Fig. 3a, as well as the spike digitization principle used in [26, 31]. Granule cells are typically studied because they constitute more than half of the neurons in the brain and, particularly, they present an exceptionally low number of synapses (four on average) [38-39] which constitutes ground for a slender electronic implementation. In neuroscience experiments, the stimulation is typically performed by applying spike trains through the mossy fibers (MFs) [40], and the experiment time is divided in temporal bins where the presence of a spike is coded as a logic 1 (0 otherwise). Fig. 3b reports the schematic of the implemented artificial neuron with the related memristor-

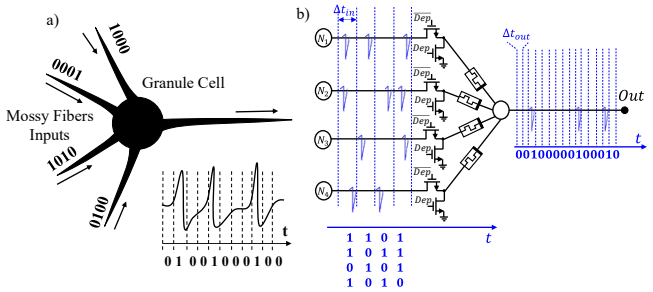

Fig. 3 – a) Example of electrical stimulation of a granule cell (4 inputs, 1 output) with mossy fiber inputs and spike digitization. b) Implementation of a biological-plausible network with 4 input neurons ($N_{1\text{-}4}$) spiking to an output neuron with memristor-based synapses. Input (output) time is divided in time bins of $\Delta t_{in} = 50ms$ ($\Delta t_{out} = 10ms$) in which the spikes are stochastically distributed.

based synapses emulating the structure on the left. Each synapse may receive up to four spikes over time, i.e., the experiment time during which the inputs are delivered to the network is composed of four temporal bins. In [26, 31] time bins of 10ms and 6ms have been used to stimulate the input and digitise the output train, respectively. Due to the technological constrains of our memristors and design choices, spikes with a longer duration are needed, which lead to define time bins of 50ms and 10ms for input and output, respectively, however with no loss of generality. As in [36, 31] we used four time bins on four inputs for the stimulation (as in Fig. 3b), giving $2^{N_{bin} \cdot N_{inputs}} = 2^{4 \cdot 4} = 65536$ possible input combinations and with a total stimulation period of 50 ms · 4 = 200ms. As explained in Section 2A, spike stimulations (10ms long) are applied at random time (jitter) within each time bins (50 ms long), consistently with the idea of digitisation of random input spike trains and with the need to introduce in an otherwise deterministic artificial network the stochastic features observed in the biological counterpart. Specifically, in-vitro experiments on GCs consist in applying specific (coded) stimuli through the neuron's MFs and repeating the experiments several times for each stimulus to sample the intrinsic neuron variability, which leads to a stochastic output. To reproduce the same stochastic response of the neuron using a deterministic neuron model, in circuit simulations each stimulus is delivered with a Poisson distributed delay (jitter) inside each time bin, therefore mimicking that the stimuli are provided by other four presynaptic neurons.

In this study we aim at quantifying how theoretical quantities related to information propagation through the network are affected by learning (i.e., plasticity on synaptic weights) to confirm analogies between biological and artificial frameworks. To do so, it is imperative to properly understand how synaptic strength is represented in the two frameworks. Indeed, although in biological experiments the synaptic efficacy (weight) is measured in terms of release probability $\bar{p}$, a stochastic parameter quantifying the synaptic strength, [26], in memristor-based neuromorphic networks the weight is represented by the memristor conductance. In fact, in biological synapses the efficacy is increased (decreased) by applying LTP (LTD) theta burst trains which, in our approach, will result in an increased (decreased) memristor conductance.

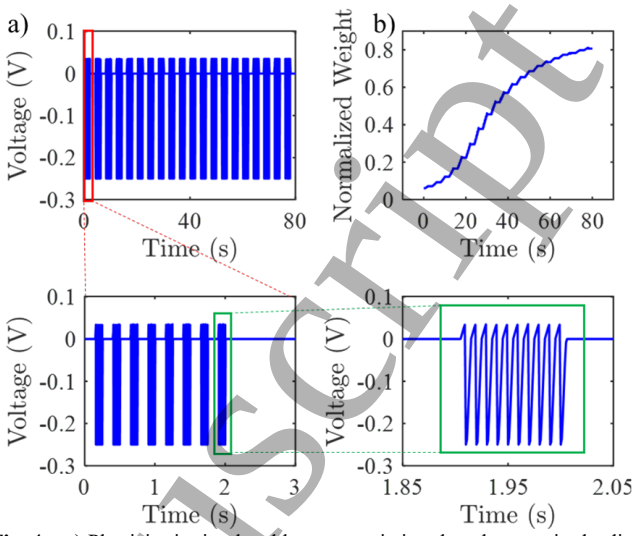

Fig. 4 – a) Plasticity is simulated by a potentiation theta burst train, leading to a conductivity change (b) which is then used to calibrate the synaptic weights of the network. In (a) the LTP theta burst sequence is reported with progressive zoom levels. In (b) the normalized weight change over time is reported when the pattern in (a) is delivered.

Therefore, in this study we simulated the system for different value of memristor conductance and we looked at how MI, Stimulus Specific Surprise (SSS) and Surprise per Spike (SpS) are affected by synaptic plasticity. To keep consistency with what observed in [26], in which the release probability was equal for all four MF synapses at the GC (i.e., any permutation of the four input was equivalent), we reduced the number of different stimuli from 65536 (all possible input combinations) to 3876 making the four synaptic inputs equal. Also, to repeat simulations for different value of memristor conductance while trying to follow bio-inspired protocols, the memristors conductance values used in simulations (and related to $\bar{p}$) have been increased in between consecutive simulations by applying specifically designed LTP theta burst (as depicted in Fig. 4a) and consequently updating the synaptic weights based on the conductance variations (Fig. 4b). For each synaptic weight, the 3876 stimuli are then delivered 15 times through the inputs and ranked on the basis of their relative SpS. As the goal of this study is to understand how information propagates through an artificial network when synaptic strength values are in a fixed configuration, we excluded possible influence of the synaptic weight variations induced by the input transmission by disabling the plasticity mechanism in the Verilog-A model of the memristor during the application of input spike trains, leaving it enabled only during the application of the theta bursts in Fig. 4. This implies that the results concerning the information transfer analysis, reported in the following Section, can be considered valid regardless of the specific device employed to represent the synaptic weights. Naturally, such a device needs to show potentiation and depression capabilities to fulfil the role of a synaptic element in a SNN. Nevertheless, information propagation through the network will show the features discussed in the following regardless of the technological specifications and of the peculiar learning features of the synaptic device.

V. Results and Discussion

It is now possible to look at the effect of synaptic plasticity on a spiking neuron with memristive synapses by analysing the key quantities related to information transfer such as entropy, MI and surprise when stimulating the network as described in Section IV.

A. Information transfer analysis

Shannon MI provides the mathematical framework to quantify the amount of information transmitted by a neuron during neural stimulation. Since our aim was to investigate whether the envisaged neuromorphic architecture could reliably reproduce neuronal performances, we explored the dependencies of MI on the synaptic efficacy (i.e., the memristor conductance). In analogy with [26, 31] the reduced number of inputs allowed to calculate MI and, as explained in the Methods section and shown in Fig. 3, we have first digitized spike trains, then a controlled set of stimuli 'S' was chosen. Secondly, responses 'r' were detected when stimuli with known a priori probabilities p(s) were repeatedly presented. Once all the data were collected, the corresponding joint probabilities $p(r|s)$, and the probability distribution of responses averaged over the stimuli $p(r)$ were estimated. The MI was computed with Eq. (1) and since in biological systems its value has been shown to change according to variations of the release probability [26], we investigated the relationship between MI and the memristor conductance, which in our assumption was the equivalent of the synaptic efficacy. Figure 5 shows the correlation between the calculated MI and the memristor conductance values. The overall information transfer is enhanced upon increase in synaptic efficacy (memristor conductance) in accordance with the expectations. Furthermore, at a visual inspection, the dependence of MI on the memristor conductance revealed a good correlation with the corresponding p-MI curve (p; release probability) obtained with both real biological and simulated neurons (see Fig. 2b, 3b in [26]). These results, beside the demonstration of the validity of this approach in mimicking neuronal information transfer, also indirectly support the close relationship between the release probability ($\bar{p}$) and memristive conductance. We were also interested in identifying stimuli that were best encoded by the electronic neuron. The stimulus specific contribution to the MI (Stimulus Specific Surprise; eq. 2) and the Surprise per spike (SpS; eq. 3) were therefore computed allowing to identify the most informative set of stimuli (Fig. 6). Specifically, for a given value of synaptic strength the network was stimulated with the 3876 inputs and the latter were then ranked by descending SpS (black curves in Fig. 6). The same procedure has been replicated for different memristor conductance values (2.6 µS, 6.2 µS, 13.6 µS), and the results are reported in Fig. 6b-c. We initially focused on the results obtained when using the lowest memristor conductance value. As shown in Fig. 6c, we identified the stimuli with the highest and lowest SpS, respectively (i.e., the blue and red markers on the bottom black curve in Fig. 6c). We then tracked how these specific stimuli changed their ranking when the simulations were repeated after synaptic potentiation

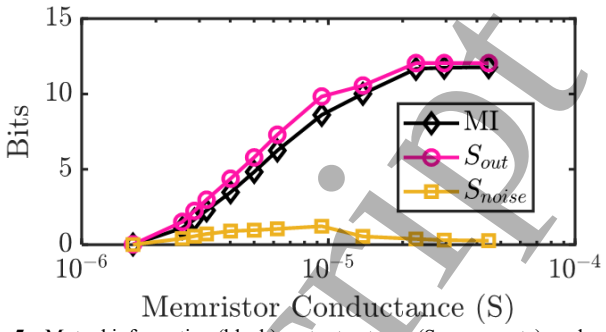

Fig. 5 – Mutual information (black), output entropy (S_{out}, magenta), and noise entropy (S_{noise}, yellow) versus memristor conductance.

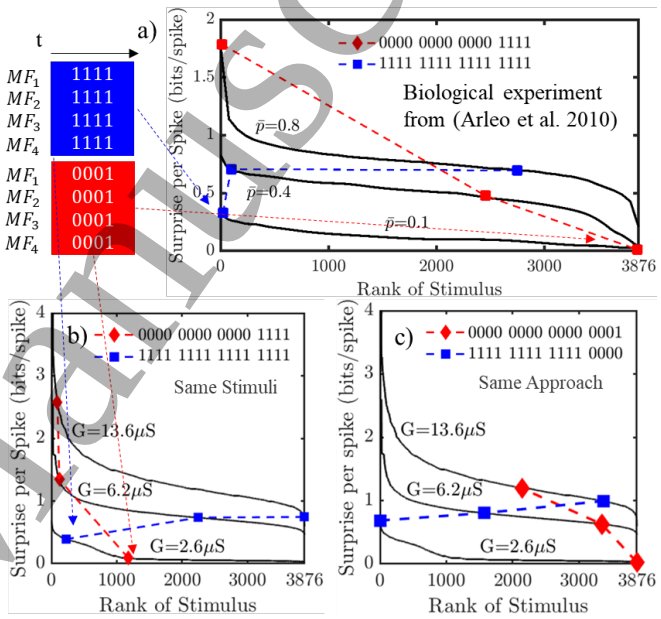

Fig. 6 – a) Surprise per spike (SpS) as a function of release probability ($\bar{p}$), adapted from [26]. The stimuli were ranked as a function of their surprise per spike for every $\bar{p}$ = 0.1-0.4-0.8. Blue and red input stimuli, consisting in the maximum and minimum SpS for the most depressed network ($\bar{p}$ = 0.1), are tracked for different p. The same experiment is reproduced in our network exploiting different synapses conductance values and tracking (b) the same stimuli as in a) and (c) using the same approach as in a), revealing similar trends.

(achieved by means of theta bursts as explained in Section IV). Both markers moved in qualitative agreement with what reported in [26], which is conveniently reported also in Fig. 6a. Although the stimuli with the highest and lowest SpS at the lowest memristor conductance were not coincident with those found in [26] at the lowest $\bar{p}$ value, the qualitative trend was found to be the same. In addition, we verified that the same trend is obtained when tracking exactly these stimuli in our simulations, as reported in Fig. 6b. Both cases confirmed the expected trends, revealing the dependability of an artificial memristor-based neuro-synaptic circuit in quantifying the information content of a specific spike train given a determined network strength.

B. Discussion

The results shown thus far confirm the similarities between a neuromorphic microcircuit composed by a neuron with a limited number of synapses endowed with a rate-based learning rule and its biological counterpart. Bio-inspired

experiments have been reproduced by assuming a dependency between the release probability and the conductance of an electronic synapse. Three parameters, namely MI, SSS, and SpS have been computed for different synaptic weights, with the aim to analyse the ability of the implemented neuron to retrieve and quantify information content from a specific stimulus based on the synaptic strength and input sparseness. Despite the differences between the neuromorphic and the biological neuron, like *i)* the noise/variability level, *ii)* the stochastic mechanisms underlying the opening of ion channels, or *iii)* the stochastic processes involved in the neurotransmitter release process, these results demonstrate from an information transmission perspective that artificial neurons can be adopted as elements performing complex computational tasks such as those performed by biological neurons. This proof of principle is a first milestone in the development of advanced neuronal networks with performance compatible with brain circuits, given their capability to compute sparse and temporally uncorrelated information. Furthermore, differently from conventional hardware, neuromorphic electronic circuit [41] can be designed to operate with a limited power consumption in multiple time domains according to circuit architectures. These advantages deriving from an electronic implementation of bio-plausible SNNs (e.g., multiple time scales and reduced area and power consumption) prove remarkably useful for different applications.

VI. Conclusions

In this work, we investigated the analogies between an artificial neuron combining memristor synapses and rate-based learning rule with biological neuron response in terms of information propagation from a theoretical perspective. Bio-inspired experiments have been reproduced by linking the biological probability of release $\bar{p}$ with the artificial synapses conductance. MI, SSS, and SpS have been computed for different synaptic weights, with the aim to analyse the ability of the implemented neuron to retrieve and quantify information content from a specific stimulus based on the synaptic strength. Results highlight that an artificial neuron allows to develop a reliable and biological resembling neural network in terms of information analysis. Advantages deriving from an electronic implementation (e.g., time scale and area) provide a remarkably useful tool for different applications.

Acknowledgment

The authors would like to thank Mr. Davide Florini for tangible support, early developments, and fruitful discussions. The work has been partially funded under the National Recovery and Resilience Plan (NRRP), Mission 04 Component 2 Investment 1.5 – NextGenerationEU, Call for tender n. 3277 dated 30/12/2021, Award Number: 0001052 dated 23/06/2022.

References

[1] Mapelli J, Gandolfi D, Vilella A, Zoli M, Bigiani A. Heterosynaptic GABAergic plasticity bidirectionally driven by the activity of pre- and postsynaptic NMDA receptors. Proc Natl Acad Sci U S A. 2016 Aug 30;113(35):9898-903. doi: 10.1073/pnas.1601194113. Epub 2016 Aug 16. PMID: 27531957; PMCID: PMC5024594.

[2] Gandolfi D, Bigiani A, Porro CA, Mapelli J. Inhibitory Plasticity: From Molecules to Computation and Beyond. Int J Mol Sci. 2020 Mar 6;21(5):1805. doi: 10.3390/ijms21051805. PMID: 32155701; PMCID: PMC7084224.

[3] Chung-Wei Wu et al., "Realizing forming-free characteristic by doping Ag into HfO2-based RRAM", 2021 Appl. Phys. Express 14 041008. DOI: 10.35848/1882-0786/abec58.

[4] Park, J., Ryu, H. & Kim, S., "Nonideal resistive and synaptic characteristics in Ag/ZnO/TiN device for neuromorphic system", Sci Rep 11, 16601 (2021). DOI: 10.1038/s41598-021-96197-8

[5] E. Covi, W. Wang, Y. -H. Lin, M. Farronato, E. Ambrosi and D. Ielmini, "Switching Dynamics of Ag-Based Filamentary Volatile Resistive Switching Devices—Part I: Experimental Characterization," in IEEE Transactions on Electron Devices, vol. 68, no. 9, pp. 4335-4341, Sept. 2021, doi: 10.1109/TED.2021.3076029.

[6] D. Florini, D. Gandolfi, J. Mapelli, L. Benatti, P. Pavan and F. M. Puglisi, "A Hybrid CMOS-Memristor Spiking Neural Network Supporting Multiple Learning Rules," in IEEE Transactions on Neural Networks and Learning Systems, 2022, doi: 10.1109/TNNLS.2022.3202501.

[7] Mario Lanza et al. "Memristive technologies for data storage, computation, encryption, and radio-frequency communication" Science 376, eabj9979(2022). DOI:10.1126/science.abj9979.

[8] W. Banerjee, "Challenges and Applications of Emerging Nonvolatile Memory Devices," Electronics, vol. 9, no. 6, p. 1029, Jun. 2020, doi: 10.3390/electronics9061029.

[9] Butts DA, Goldman MS. Tuning curves, neuronal variability, and sensory coding. PLoS Biol. 2006 Apr;4(4):e92. doi: 10.1371/journal.pbio.0040092. Epub 2006 Mar 21. PMID: 16529529; PMCID: PMC1403159

[10] Kang K, Shapley RM, Sompolinsky H. Information tuning of populations of neurons in primary visual cortex. J Neurosci. 2004 Apr 14;24(15):3726-35. doi: 10.1523/JNEUROSCI.4272-03.2004. PMID: 15084652; PMCID: PMC6729344.

[11] J Mapelli, GM Boiani, E D'Angelo, A Bigiani, D Gandolfi, "Long-Term Synaptic Plasticity Tunes the Gain of Information Channels through the Cerebellum Granular Layer", Biomedicines 10 (12), 3185

[12] Barak O, Rigotti M, Fusi S. The sparseness of mixed selectivity neurons controls the generalization-discrimination trade-off. J Neurosci. 2013 Feb 27;33(9):3844-56. doi: 10.1523/JNEUROSCI.2753-12.2013. PMID: 23447596; PMCID: PMC6119179.

[13] Rigotti M, Barak O, Warden MR, Wang XJ, Daw ND, Miller EK, Fusi S. The importance of mixed selectivity in complex cognitive tasks. Nature. 2013 May 30;497(7451):585-90. doi: 10.1038/nature12160. Epub 2013 May 19. PMID: 23685452; PMCID: PMC4412347.

[14] LF. Abbott and P Dayan Theoretical Neuroscience Computational and Mathematical Modeling of Neural Systems the MIT press October 26, 2001

[15] Quian Quiroga R, Panzeri S. Extracting information from neuronal populations: information theory and decoding approaches. Nat Rev Neurosci. 2009 Mar;10(3):173-85. doi: 10.1038/nrn2578. PMID: 19229240.

[16] Bialek W, Rieke F, de Ruyter van Steveninck RR, Warland D. Reading a neural code. Science. 1991 Jun 28;252(5014):1854-7. doi: 10.1126/science.2063199. PMID: 2063199.

[17] London M, Schreibman A, Häusser M, Larkum ME, Segev I. The information efficacy of a synapse. Nat Neurosci. 2002 Apr;5(4):332-40. doi: 10.1038/nn826. PMID: 11896396.

[18] Shannon C. The Mathematical Theory of Communication. The Bell System technical Journal. 1948; 27: 379–423.

[19] Borst A, Theunissen FE. Information theory and neural coding. Nat Neurosci. 1999; 2(11): 947–57. pmid:10526332

[20] Panzeri S, Senatore R, Montemurro MA, Petersen RS. Correcting for the sampling bias problem in spike train information measures. J Neurophysiol. 2007; 98(3): 1064–72. pmid:17615128

[21] B. Joo, J. -W. Han and B. -S. Kong, "Energy- and Area-Efficient CMOS Synapse and Neuron for Spiking Neural Networks With STDP Learning," in IEEE Transactions on Circuits and Systems I: Regular Papers, vol. 69, no. 9, pp. 3632-3642, Sept. 2022, doi: 10.1109/TCSI.2022.3178989.

[22] T. Guo et al., Adjustable Leaky-Integrate-and-fire neurons based on memristor-coupled capacitors, Materials Today Advances, Volume 12, 2021, 100192, ISSN 2590-0498, doi: 10.1016/j.mtadv.2021.100192.

[23] John, R.A., Demirağ, Y., Shynkarenko, Y. et al. Reconfigurable halide perovskite nanocrystal memristors for neuromorphic computing. Nat Commun 13, 2074 (2022). doi: 10.1038/s41467-022-29727-1.

[24] Kumar, S., Wang, X., Strachan, J.P. et al. Dynamical memristors for higher-complexity neuromorphic computing. Nat Rev Mater 7, 575–591 (2022). doi: 10.1038/s41578-022-00434-z

[25] S. Anwer et al., Cobalt oxide nanoparticles embedded in borate matrix: A conduction mode atomic force microscopy approach to induce nano-memristor switching for neuromorphic applications, Applied Materials Today, Volume 29, 2022, 101691, ISSN 2352-9407, https://doi.org/10.1016/j.apmt.2022.101691.

[26] Arleo A, Nieus T, Bezzi M, D'Errico A, D'Angelo E, Coenen OJ. How synaptic release probability shapes neuronal transmission: information-theoretic analysis in a cerebellar granule cell. Neural Comput. 2010; 22(8): 2031–58. pmid:20438336

[27] Casali S, Tognolina M, Gandolfi D, Mapelli J, D'Angelo E. Cellular-resolution mapping uncovers spatial adaptive filtering at the rat cerebellum input stage. Commun Biol. 2020 Oct 30;3(1):635. doi: 10.1038/s42003-020-01360-y. PMID: 33128000; PMCID: PMC7599228.

[28] Mapelli J, Gandolfi D, Giuliani E, Casali S, Congi L, Barbieri A, D'Angelo E, Bigiani A. The effects of the general anesthetic sevoflurane on neurotransmission: an experimental and computational study. Sci Rep. 2021 Feb 22;11(1):4335. doi: 10.1038/s41598-021-83714-y. PMID: 33619298; PMCID: PMC7900247.

[29] Nieus T, Sola E, Mapelli J, Saftenku E, Rossi P, D'Angelo E. LTP regulates burst initiation and frequency at mossy fiber-granule cell synapses of rat cerebellum: experimental observations and theoretical predictions. J Neurophysiol. 2006 Feb;95(2):686-99. doi: 10.1152/jn.00696.2005. Epub 2005 Oct 5. PMID: 16207782.

[30] Gandolfi D, Pozzi P, Tognolina M, Chirico G, Mapelli J, D'Angelo E. The spatiotemporal organization of cerebellar network activity resolved by two-photon imaging of multiple single neurons. Front Cell Neurosci. 2014 Apr 15;8:92. doi: 10.3389/fncel.2014.00092. PMID: 24782707; PMCID: PMC3995049.

[31] Mapelli J, Gandolfi D, Giuliani E, Prencipe FP, Pellati F, Barbieri A, D'Angelo E, Bigiani A. The effect of desflurane on neuronal communication at a central synapse. PLoS One. 2015 Apr 7;10(4):e0123534. doi: 10.1371/journal.pone.0123534. PMID: 25849222; PMCID: PMC4388506.

[32] F.M. Puglisi, T. Zanotti and P. Pavan, "Unimore Resistive Random Access Memory (RRAM) Verilog-A Model," nanoHUB, Jun 2019, doi: 10.21981/15GF-KX29.

[33] A. Padovani, L. Larcher, F. M. Puglisi and P. Pavan, "Multiscale modeling of defect-related phenomena in high-k based logic and memory devices," in 2017 IEEE 24th International Symposium on the Physical and Failure Analysis of Integrated Circuits (IPFA), Jul. 2017, pp. 1–6, doi: 10.1109/IPFA.2017.8060063

[34] T. Zanotti, P. Pavan, F.M. Puglisi, "Comprehensive physics-based RRAM compact model including the effect of variability and multi-level random telegraph noise", Microelectronic Engineering, Volume 266, 2022, 111886, ISSN 0167-9317, https://doi.org/10.1016/j.mee.2022.111886.

[35] F. M. Puglisi, N. Zagni, L. Larcher and P. Pavan, "Random Telegraph Noise in Resistive Random Access Memories: Compact Modeling and Advanced Circuit Design," in IEEE Transactions on Electron Devices, vol. 65, no. 7, pp. 2964-2972, July 2018, doi: 10.1109/TED.2018.2833208

[36] K.A. Campbell, "Self-directed channel memristor for high temperature operation," in Microelectronics Journal, vol. 59, Jan. 2017, pp. 10-14, doi: 10.1016/j.mejo.2016.11.006.

[37] S. S. Chowdhury, C. Lee, K. Roy, "Towards understanding the effect of leak in Spiking Neural Networks", Neurocomputing, Volume 464, 13 November 2021, Pages 83-94. DOI: 10.1016/j.neucom.2021.07.091.

[38] Eccles, J. C., Ito, M., and Szentagothai, J. (1967). The Cerebellum as a Neuronal Machine. Berlin: Springer Verlag.

[39] Jakab RL, Hámori J. Quantitative morphology and synaptology of cerebellar glomeruli in the rat. Anat Embryol (Berl). 1988;179(1):81-8. doi: 10.1007/BF00305102. PMID: 3213958.

[40] Chadderton P, Margrie TW, Häusser M. Integration of quanta in cerebellar granule cells during sensory processing. Nature. 2004; 428: 856–860. pmid:15103377

[41] Gandolfi D, Puglisi FM, Boiani GM, Pagnoni G, Friston KJ, D'Angelo E, Mapelli J. Emergence of associative learning in a neuromorphic inference network. J Neural Eng. 2022 May 30;19(3). doi: 10.1088/1741-2552/ac6ca7. PMID: 35508120.